Directional eye fixation sensor using birefringence-based foveal detection

Boris I. Gramatikov, Othman H. Y. Zalloum, Yi Kai Wu, David G. Hunter, and David L. Guyton

We recently developed and reported an eye fixation monitor that detects the fovea by its radial orientation of birefringent nerve fibers. The instrument used a four-quadrant photodetector and a normalized difference function to check for a best match between the detector quadrants and the arms of the bow-tie pattern of polarization states surrounding the fovea. This function had a maximum during central fixation but could not tell where the subject was looking relative to the center. We propose a linear transformation to obtain horizontal and vertical eye position coordinates from the four photodetector signals, followed by correction based on *a priori* calibration information. The method was verified on both a computer model and on human eyes. The major advantage of this new eye-tracking method is that it uses true information coming from the fovea, rather than reflections from other structures, to identify the direction of foveal gaze.

OCIS codes: 330.4460, 170.3890, 330.2210, 200.4560, 260.1440, 260.5430.

1. Introduction

There is an increasing demand for accurate, noninvasive eye trackers. When an individual looks at a target, that target is imaged onto the fovea. This foveal fixation correlates with gaze direction and eye position. Eye position can be estimated by a variety of techniques, each having advantages and limitations.[1–9]

Electromagnetic induction methods utilizing a search coil require a scleral contact lens.[1,2,10] Other eye trackers follow relative positions of pupillary images or of the Purkinje light reflexes.[3,5,6,11,12] Scleral reflection trackers require head-mounted emitters and detectors for monitoring changes in scleral reflectance induced by eye movements.[7] In the past 7 years or so, the advent of CCD and complementary metal-oxide semiconductor (CMOS) cameras has led to the miniaturization of video-based systems.[9,11,12] Flying-spot scanning technologies, which selectively image landmarks on the eye, have improved precision, but this precision comes at the cost of interference from specular reflections, reduced speed, and limited life of the beam-steering system consisting of galvanometer-driven mirrors.[8] For research purposes, most studies have used head-mounted eye-tracking devices, but more recently remote systems have been applied as well.[11,13]

Some of the existing commercial systems are fast and can operate in real time at high frame rates, such as the Chronos system (Berlin, Germany),[9] the El Mar (Downsview, Ontario) eye tracker,[14] and the Applied Science Laboratories (Bedford, Massachusetts) Models 501 and 504.[13] The most prevalent approach for gaze direction detection with most commercial systems available today appears to be the indirect method of determining corneal light reflex position versus pupil position.[11,12,14] It seems that it has not been possible until now to detect true foveal fixation remotely, continuously, and noninvasively.

Polarized near-infrared light is reflected from the foveal area in a bow-tie pattern of polarization states similar to the Haidinger brush phenomenon.[15] In the late 1980s, human foveal birefringence was measured *in vivo* with Mueller-matrix ellipsometry.[16] In the early 1990s, the birefringence of the retinal nerve fibers was utilized by Dreher *et al.*[17] to measure the thickness of the nerve fiber layer. Based on this, Guyton and coauthors reasoned that the birefringence of the nerve fibers surrounding the human fovea (Henle fibers) might be used to detect the strict radial geom-

B. I. Gramatikov (bgramat@jhmi.edu), O. H. Y. Zalloum, Y. K. Wu, D. G. Hunter, and D. L. Guyton are with the Krieger Children's Eye Center at the Wilmer Institute, the Johns Hopkins University School of Medicine, 600 North Wolfe Street, Baltimore, Maryland 21287-9028. D. G. Hunter is also with the Department of Ophthalmology, Children's Hospital Boston, Ophthalmology-Fegan 4, 300 Longwood Avenue, Boston, Massachusetts 02115.

Received 28 April 2006; revised 29 September 2006; accepted 6 October 2006; posted 6 October 2006 (Doc. ID 70427); published 13 March 2007.

0003-6935/07/101809-10$15.00/0

etry of the nerve fibers in the fovea. Such a technique was developed by our group to monitor foveal fixation[18–20] and to detect proper alignment of the two eyes in infants and young children[21–23] for the purpose of vision screening.

Using the eye in an autoconjugate arrangement, these instruments employed a circular scanning system. When the eye is focused in the same plane as the intended fixation point (a light source in the center of the circular scan), the light reflected from the retinal scan would automatically be focused by the eye back to the source, where it could be deflected by a beam splitter and measured for changes in polarization state induced by double passage through the Henle fibers. When the eye is looking at the intended fixation point, the circular scan is centered on the bow tie of polarization states, and the change in the detected polarization state of the light is at twice the frequency of the scan, or at $2f$. With paracentral fixation, however, the change in the detected polarization state is only at the frequency of scan f.

The rapidly spinning motor, however, added noise and vibration and was generally of limited life. To avoid these problems, we developed a no-moving-parts eye fixation monitor. Instead of circular scanning, this instrument utilizes four spots of linearly polarized light to obtain spatial information. With central fixation, two spots are aligned with the bright arms, and two are aligned with the dark arms of the bow-tie pattern of polarization states surrounding the fovea. The light reflected from the fundus travels through a quarter-wave plate, a polarizer, and onto a four-quadrant photodetector. After amplification and digitization, the signals from the four photodetectors are combined into a normalized differential (ND) signal that discriminates between central fixation and the lack thereof. At central fixation the ND reaches its global maximum, which allows it to be used in conjunction with a threshold for detecting central fixation.[24] The simple ND measure can tell whether the subject is looking at the intended fixation point but cannot provide information as to exactly where the subject is looking if not centered on the intended fixation point. To solve this problem, we propose a method for calculating the x and y coordinates of the point of fixation from the data received by the four-quadrant photodetector, using the same device.

2. System Overview and Methods

A. Instrument Design and Theory of Operation

The instrument design has been reported in more detail in a previous paper.[24] To obtain better symmetry of the bow-tie pattern and the light spots with respect to the photodetector, for the purpose of eye tracking, in the present design we rotated the quadrant photodetector 45° clockwise around its center, such that the four reflected patches of light now fall on the intersections between adjacent quadrants of the photodetector. The new configuration is shown in Fig. 1. The four spots are produced from a single 780 nm, 100 mW laser diode by using a multifaceted prism. The laser is modulated by a square wave ($f = 140$ Hz). The intensity of light is safe for exposure times of up to 3×10^4 s.[25] The incident light is vertically polarized. The radially oriented retardance around the fovea induces a circularly polarized component in the reflected beam. The light reflected from the fundus travels through a circular analyzer (quarter-wave plate followed by a linear polarizer), which produces four patches of light as parts of a bow-tie intensity pattern. These spots are captured by a quadrant photodetector extending over 4° of visual angle (Centrovision QD50-0, active area 8 mm diameter). For the reader familiar with polarization optics, we measure a portion of the S_3 component[26,27] of the polarization state of each reflected patch of light. In the Stokes vector representation of the polarization state, $S = \{S_0, S_1, S_2, S_3\}$, S_3 represents the differential measurement of the circular polarization component (right-handed circular polarization minus left-handed circular polarization). In our device, we measure the portion of the circular polarization component by first rotating the polarization states on the Poincaré sphere 90° by means of the quarter-wave plate, and then measuring the (nondifferential) linear polarization along the S_1 axis using a polarizer in front of the detector.

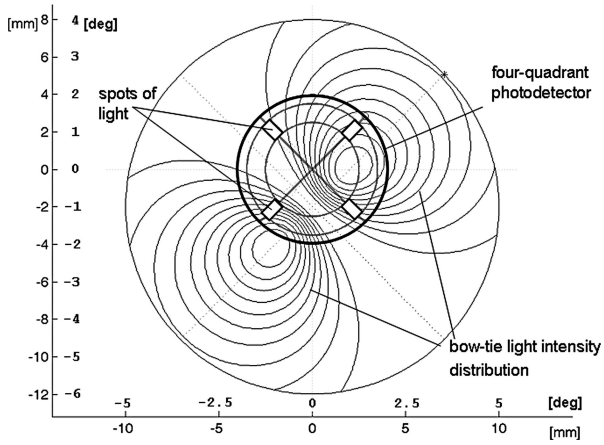

Fig. 1. Idealized 2D spatial intensity profile of the light reflected from the fundus and falling on the plane of the quadrant photodetector, if linearly polarized light were uniformly illuminating the fundus. We use only four spots of illumination, however, and the signal in each detector quadrant is calculated by integrating the intensity signal pointwise for the illuminated (rectangular) area corresponding to each spot of light.

The optical design uses a circular exit pupil of 30 mm diameter. As long as the eye is within the exit pupil, the foveal position can be measured with regard to the four spots illuminating the Henle fibers. This means that the system will tolerate horizontal and vertical displacements of the eye within the exit pupil of 30 mm diameter without loss of precision, as well as forward and backward displacements of the eye of at least ± 2 cm.

The four signals from the four photodetectors are amplified, filtered, and fed to a computer for analog-to-digital conversion and digital analysis. Signal pro-

cessing includes bandpass digital filtering at a central frequency equal to laser modulation frequency, synchronous signal averaging, and background subtraction in each of the four channels. A background measurement, arising from lid and facial reflections, as well as from internal instrument reflections, is taken with eyes closed prior to each set of fixation measurements and is stored separately for each channel for subsequent subtraction from the readings in that channel.

B. Computer Model

We developed in MATLAB a mathematical model that helps to optimize the eye-position detection algorithm.[24] The graphic output of the model is shown in Fig. 1. It represents an idealized 2D spatial intensity profile of the polarization-altered light reflected from the fundus, after passing through the quarter-wave plate and polarizer overlying the detector. The signal in each detector quadrant is calculated by integrating the light intensity pointwise across the area captured by each particular detector quadrant. Because this design employs four spots of light on the retina, the model uses a mask, thus sensing only light reflected by the four spots directly illuminated by the laser diode. All other parts of the retina are masked out. The spots of light are conjugate to the intersections between adjacent quadrants of the photodetector (Fig. 1) but are reflected from different areas of the fovea depending on the actual point of fixation. For simplicity, this model does not take into account the blurring that occurs due to imperfect imaging in the double pass. It rather behaves as if a four-quadrant detector were placed immediately above the retina on the return path.

As reported in more detail in our previous paper,[24] the bow-tie distribution of light intensities, upon passing through the polarizer overlying the quadrant detector, was modeled with a $\cos^2(\theta)$ function where θ is the azimuth of the fast axis of the Henle fiber birefringence, radially disposed with respect to the center of the bow tie. This function was modulated with an exponentially rising and then exponentially falling radial function derived from previous measurements in our laboratory.[28] This exponential function has a peak at approximately 1.5° of visual angle. The product of the two functions gives the bow-tie pattern shown in Fig. 1, where the two peaks are approximately 3° (6 mm in terms of detector space) apart, and represents the areas of maximum change in polarization state (S_3 component measured) coming from the fovea.

Depending on the direction of gaze, different portions of the bow-tie intensity pattern are projected onto the four quadrants of the photodetector. In the model, the center of the bow-tie intensity pattern can be positioned at any point in the plane of the photodetector. For each position of the bow-tie center (point x, y) the model yields a set of signals [A, B, C, D] corresponding to the signals received from the four detector segments of the four-quadrant photodetector. We aligned the coordinate system X'–Y' with the axis of the foveal bow-tie light intensity pattern (Fig. 2), as tilted at an angle ψ with respect to the normal Cartesian system X–Y, whereby the tilt angle ψ could be set to an arbitrary value. In reality, the bow-tie orientation depends on the polarization properties of the incident beam, as well as on the birefringence of the cornea. For a vertically polarized incident beam, as in our system, an orientation of 45° occurs when the corneal retardance is equal to zero. The influence of the retardance and azimuth of the corneal birefringence on the orientation of the bow tie was studied in our previous paper.[24]

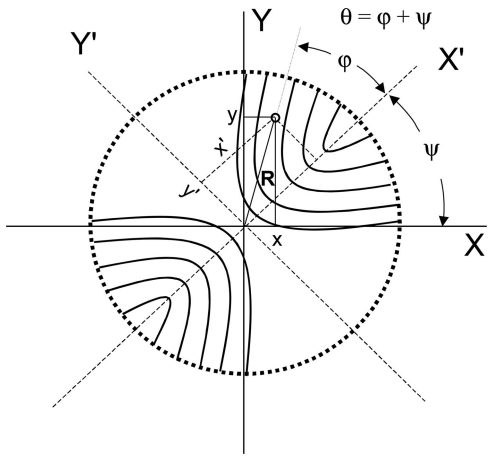

Fig. 2. Coordinate system X'–Y' of the foveal bow-tie light intensity pattern (after passing through the quarter-wave plate and polarizer) as tilted at an angle ψ with respect to the normal Cartesian system X–Y($\psi \approx 45°$).

C. Eye-Tracking Equation in the Computer Model

We assume that for each position of the eye there exists a set of parameters [v, w] such that

$$[A \quad B \quad C \quad D]\begin{bmatrix} v_1 & w_1 \\ v_2 & w_2 \\ v_3 & w_3 \\ v_4 & w_4 \end{bmatrix} = [x \quad y], \tag{1}$$

or $\mathbf{aV} = \mathbf{u}$, where $\mathbf{u} = [x, y]$ is the known position vector, $\mathbf{a} = [A, B, C, D]$ is the known detector output, and $\mathbf{V} = [v, w]$ is an unknown transformation matrix containing four v elements and four w elements.

We hypothesize that, with reasonable precision, one and the same set of transformation parameters $\mathbf{V}$ can be applied to the linear calculation of the coordinates of the bow-tie center (eye position with respect to the center of the four-quadrant photodetector) for all the positions of the bow tie within a certain range, and that $\mathbf{V}$ can be optimized so as to minimize the overall error. Further, we hypothesize that the calculation error attributable to deviation from this linear model can be reversed by using *a priori* correction information obtained after calibration but before real-time operation.

To find $\mathbf{V}$, the model can be used to move the center of the bow-tie intensity pattern about on a grid

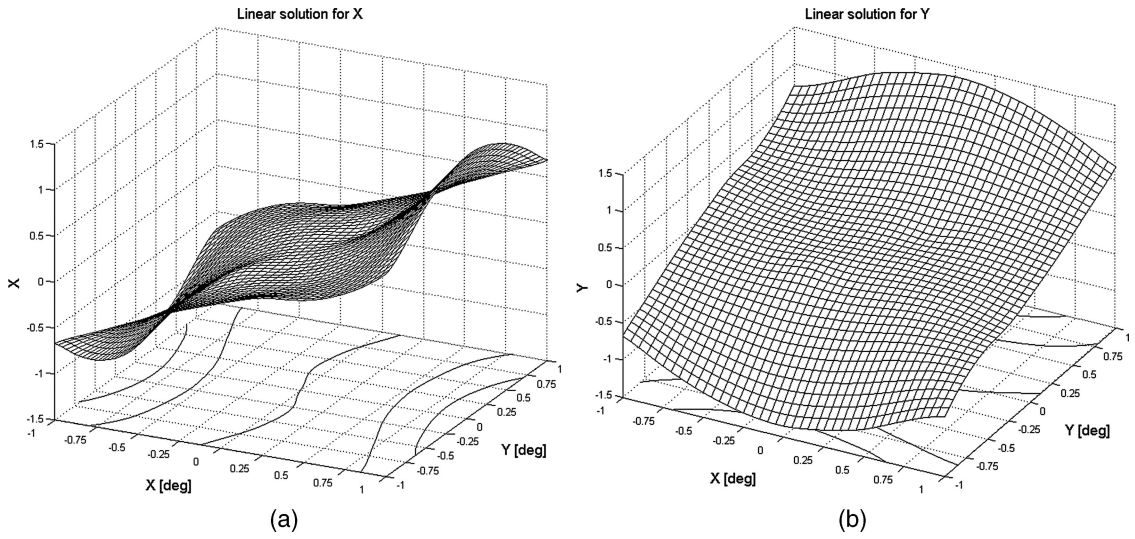

Fig. 3. Modeling eye tracking: linear solution, the backcalculated signal for (a) X and (b) Y after computing the transformation matrix $\mathbf{V}$ and applying it to the input data (A, B, C, D) for each point.

(g-by-h) with respect to the detector center, and the detector output $\mathbf{a}_i = [A_i, B_i, C_i, D_i]$ can be obtained for each position (observation). For all n observations ($n = g * h$) we can then write the following set of simultaneous linear equations:

$$\mathbf{AV} = \mathbf{U}, \tag{2}$$

where $\mathbf{A}$ is an n-by-4 observation matrix, $\mathbf{V}$ is a 4-by-2 transformation matrix, and $\mathbf{U}$ is an n-by-2 eye-position matrix. For $n > 4$ matrix $\mathbf{A}$ is rectangular and the system is an overdetermined one. Matrix $\mathbf{A}$ is factored using QR orthogonalization. The factors are used to solve the overdetermined equations in a least-squares sense. The result is a q-by-r matrix where q ($q = 4$) is the number of columns of $\mathbf{A}$, and r ($r = 2$) is the number of columns of $\mathbf{U}$. Each column of $\mathbf{V}$ has at most k nonzero components, where k is the effective rank of $\mathbf{A}$. In our case of n-by-4, $\mathbf{A}$ generally has $k = n$ (full rank). The solution for $\mathbf{V}$ can be given as

$$\mathbf{V} = \mathrm{pinv}(\mathbf{A}) * \mathbf{U}, \tag{3}$$

where the pinv operator finds the pseudoinverse matrix. To solve Eq. (3) we used MATLAB. Further, to examine the efficiency of the computed transformation matrix $\mathbf{V}$, we calculated backward $\mathbf{u}_c = [x, y]$ as a linear solution using Eq. (1) for each of the n observations from the grid ($n = g * h$). The grid stretched from $-1°$ to $+1°$ in both x and y directions and had $9 \times 9 = 81$ nodes (Fig. 3).

D. Eye-Tracking Equation with Human Data

In a similar manner, we analyzed the data collected from human eyes. Four male adults, aged 23–60, were tested. The study was approved by the Institutional Review Board for all the measurements described here, and written consent was obtained from each subject. The subjects had no history of eye disease and had corrected visual acuity of 20/20 or better in the tested eye. We prepared a special 2D eccentric viewing scale for the fixation detector and reflected it via a beam splitter in the test subject's visual field, centered on the central fixation point, in a way that allowed the subject to fixate on any intersection of the grid, at known coordinates relative to the center of the four red dots. Each measurement was background corrected, and the average of five measurements was used for each point. During measurement, we recorded $\mathbf{a}_i = [A_i, B_i, C_i, D_i]$ and $\mathbf{u}_i = [x_i, y_i]$ for each grid intersection, as in Eq. (1), obtaining for n nodes (grid intersections) a relationship as in Eq. (1). Then using Eq. (3), we calculated the transformation matrix $\mathbf{V}$ and calculated backward $\mathbf{u}_c = [x, y]$ using Eq. (1) for each observation from the grid.

E. Correction of the Linear Solution Using Calibration Information

For some applications, a directional eye fixation sensor based solely on a linear solution, as given in Eq. (1), may be sufficient. For more demanding applications, we propose a correction algorithm based on correction matrices for X and Y, respectively. In this case, data acquired during calibration are used first to compute the transformation matrix $\mathbf{V}$ and to calculate backward for all calibration nodes $\mathbf{u}_c = [x, y]$ using Eq. (1), as described in Subsections 2.C and 2.D. We call these backcalculated pairs estimates of the real coordinates, i.e., x_{est} and y_{est}. To each pair of real coordinates $[x, y]$ and for a given transformation matrix $\mathbf{V}$, there is a corresponding pair of estimated coordinates x_{est} and y_{est}. Conversely, we observed in the computer model and in the human data that no two $[x, y]$ pairs produced the same $[x_{est}, y_{est}]$ pair or a set of pairs too close to each other. This allowed us to invert the plots for the estimated linear solutions x_{est} and y_{est} (Figs. 3 and 6) and, after resampling of the error, to present them as correction matrices (Figs. 4

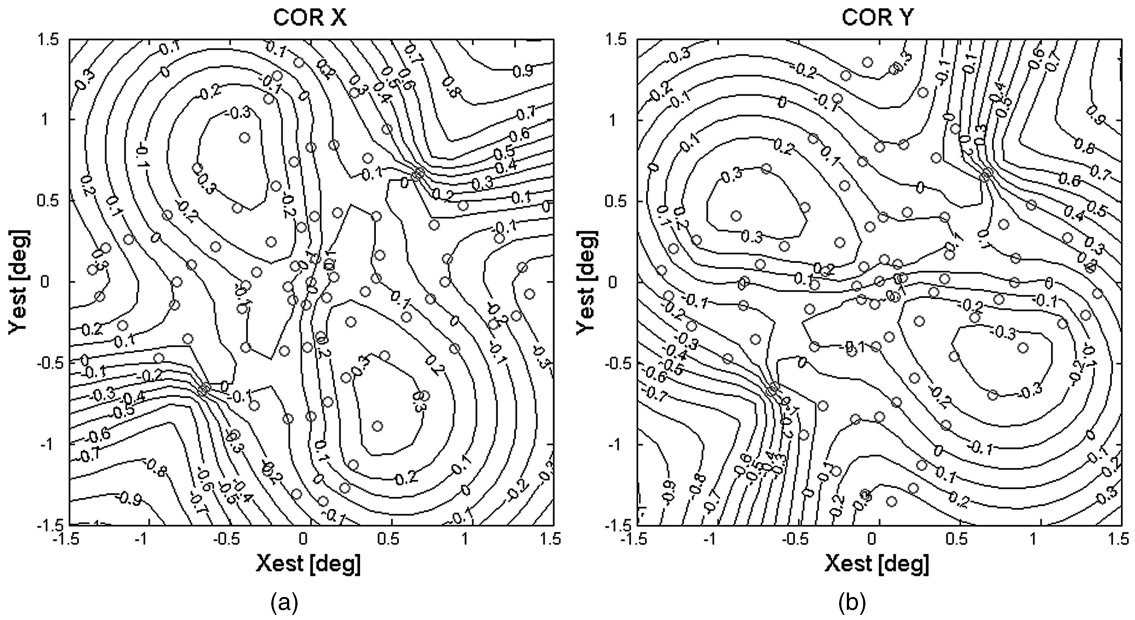

Fig. 4. Modeling eye tracking: resampled correction matrices for (a) X and (b) Y. Circles indicate data from nodes on the original grid.

and 7) for X and Y. Resampling was done on a regular grid by using spline interpolation.[29] During real-time operation, each correction matrix **COR_X** and **COR_Y** (for X or Y, respectively) is entered with the linearly estimated pair $[x_{est}, y_{est}]$ and delivers the correction value for X or Y, respectively. Since entry into a correction matrix is possible only for discrete values of x_{est} and y_{est}, one should use either high-density matrices (finer grid cells) and approximate before entry, or, alternatively, interpolate the output value in real time between the closest surrounding nodes (control points) of the correction matrix. We chose the second approach, to compute the output using an inverse distance-squared interpolation equation based on the values for the four corner (control) points of the matrix grid cell into which the current input falls:

$$Z_k = \frac{\sum_{i=1}^{4}\left(\frac{Z_i}{D_{ik}^{\,2}}\right)}{\sum_{i=1}^{4}\frac{1}{D_{ik}^{\,2}}}, \qquad D_{ik} = [(x_k - x_i)^2 + (y_k - y_i)^2]^{1/2}. \quad (4)$$

In Eqs. (4), Z is the final interpolated correction value for either X or Y. This method is faster and computationally simpler than the spline interpolation, while yielding satisfactory results.

3. Results

A. Eye Tracking in the Computer Model

We ran the model described in Subsection 2.B, with the mutual positions of the bow-tie light intensity pattern and detector being shifted by the program with a step of 0.25° in each direction (X, Y). We worked in the coordinate system X'–Y' of the foveal bow-tie light intensity pattern (Fig. 2), as tilted at an angle $\psi = 45°$ with respect to the normal Cartesian system X–Y. In the rotated X'–Y' system the X' axis runs through the middle of the areas of maximum change in polarization state (S_3 component) coming from the fovea, whereas the Y' axis halves the areas of minimum birefringence signal. The transformation from one system to another, rotated at an angle ψ was done using the equations

$$R = \sqrt{x'^2 + y'^2}, \qquad \varphi = a\tan\left[\frac{y'}{x'}\right], \qquad \vartheta = \varphi + \psi,$$
$$x = R\cos(\vartheta), \qquad y = R\sin(\vartheta). \quad (5)$$

For transformations from the normal X–Y system to the foveal X'–Y' system, we used $\psi = -45°$, and for the inverse transformation X'–Y' to X–Y system, accordingly $\psi = 45°$.

The four quadrant signals A, B, C, and D were calculated for each position in X'–Y' and used for computing the transformation matrix **V** according to Eqs. (2) and (3). Here the known position vector **u** of Eq. (1) is in the foveal bow-tie coordinate system. Then the values for X' and Y' were backcalculated, returned to the original normal coordinate X–Y system [Eq. (5), $\psi = 45°$], and plotted for each position after interpolation on a finer grid (Fig. 3). For the whole field studied, it can be seen for the simple linear solution that the X measure gradually increases from left to right on the X plots [Fig. 3(a)], and the Y measure similarly increases from down to up on the Y plots [Fig. 3(b)]. There is also a central area of approximately 1.0° × 1.0° where the coordinates returned by the linear calculation closely match the original offsets and change nearly linearly with them in both the x and the y directions. Yet outside the central region the error increases significantly. The correction matrices **COR_X** [Fig. 4(a)] and **COR_Y**

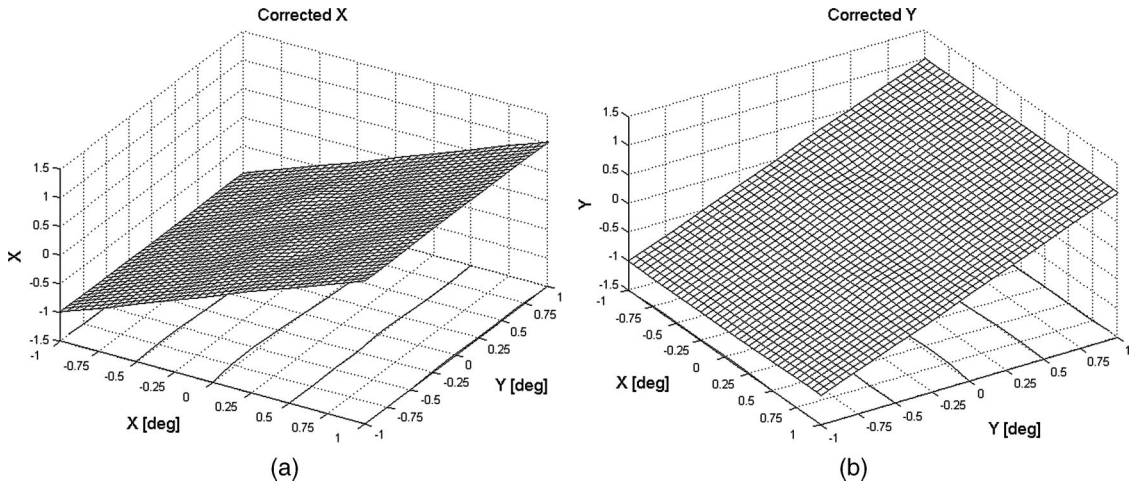

Fig. 5. Modeling eye tracking: the corrected signals for (a) X and (b) Y after XY matrix correction.

[Fig. 4(b)] improve precision, rendering the corrected x and y excellent linear functions of the original direction of gaze $[x, y]$ (Fig. 5). The absolute error after matrix-based correction does not exceed 0.03° for either X or Y, which is 1.5% of the size of the whole field studied.

B. Eye Tracking in Human Subjects

Using the technique described in Subsection 2.D, we collected data from the right eyes of three properly consenting human subjects, using a 2D eccentric viewing scale. Concordant with the results in Subsection 3.A, data were obtained from the central area of $2° \times 2°$, in the range $[-1.0° \cdots + 1.0°]$ for both the x and the y directions. As in Subsection 3.A, the coordinates were first converted to the coordinate system X'–Y' of the foveal bow-tie light intensity pattern. Then based on the known position vector $\mathbf{u} = [x, y]$ used for fixation when collecting data from different spots on the eccentric scale, for each subject the transformation matrix $\mathbf{V}$ was calculated [Eq. (3)], and for each observation the predicted position vector $\mathbf{u}_c = [x, y]$ was backcalculated [Eqs. (1 and 2)]. Finally, computed coordinates were returned to the original X–Y coordinate system [Eq. (5), $\psi = 45°$]. The results for X and Y for one of the subjects are presented in Fig. 6.

For the linear solution applied to different points on the field studied, it can be seen on the plots for X [Fig. 6(a)] that the x function increases monotonically from left to right, although this rise is not the same for different values of Y. Similarly, the plots for Y [Fig. 6(b)] show a function generally proportional to the y coordinate, but the rate of increase depends on the x position. Although the functions for X and Y are monotonic, linearity exists only in the central region and deteriorates toward the corners of the field studied. The linear error for X can be as high as 0.7°, which is 35% of the field size, and the error for Y can reach 0.5°, equivalent to 25% of the field size in the border areas. Such precision may be good only for very unchallenging applications (like actuating big

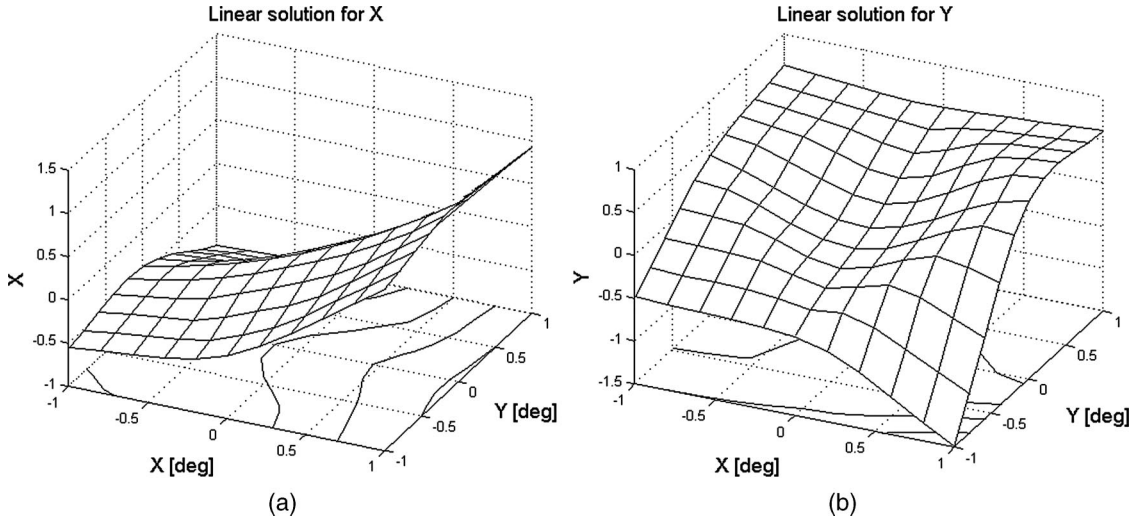

Fig. 6. Eye tracking with human data: linear solution, the backcalculated signal for (a) X and (b) Y after computing the transformation matrix $\mathbf{V}$ and applying it to the input data (A, B, C, D) for each point.

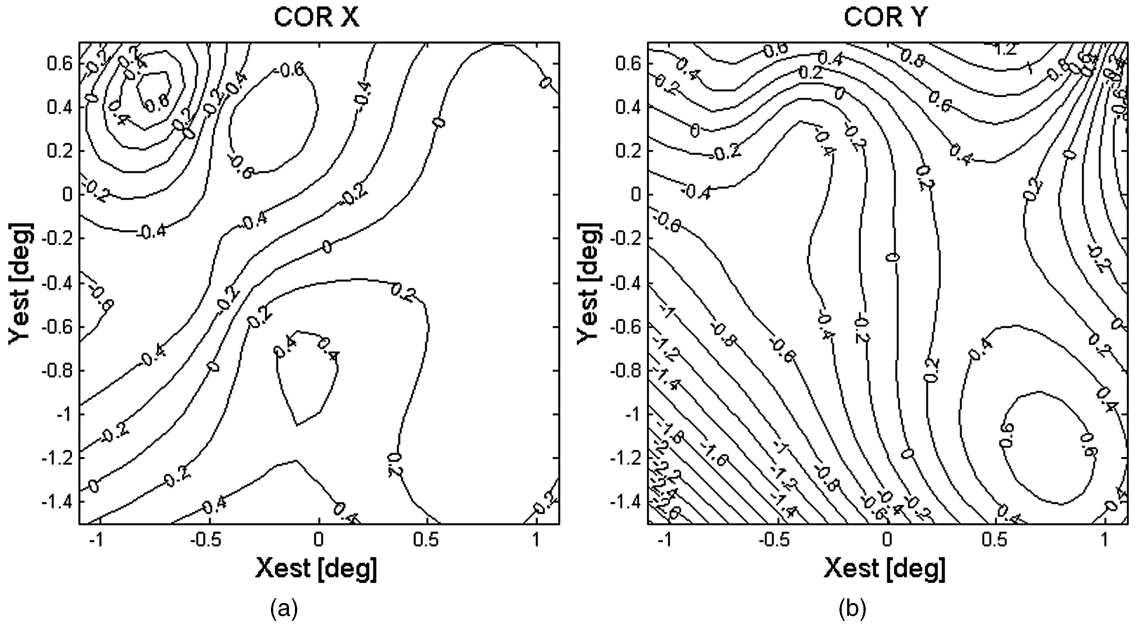

Fig. 7. Eye tracking with human data: resampled correction matrices for (a) X and (b) Y.

visual buttons), but is obviously insufficient for more demanding tasks. The correction matrices **COR_X** [Fig. 7(a)] and **COR_Y** [Fig. 7(b)] improve precision considerably, resulting ultimately, as with the model, in very good linear behavior of both X and Y [Figs. 8(a) and 8(b)]. The absolute error after matrix-based correction amounts to less than 0.09° for X and less than 0.05° for Y, which are 4.5% and 2.5% of the size of the whole field, respectively. All four tested subjects performed similarly, with the error not exceeding 0.11° for X and 0.08° for Y (5.5% and 4.0% relative to the field size, respectively).

Additional tests on the human data, as well as on the model, showed that computing the transformation matrix **V** without converting the coordinates to and from the coordinate system X'–Y' did not significantly change the precision of the x and y estimations. This has the useful implication that the tilt angle ψ of the foveal brush, which is approximately 45° but may vary somewhat from patient to patient, would not significantly influence the precision of the gaze detection.

4. Discussion and Limitations

The results support our initial hypothesis that the direction of gaze can be determined from the four quadrant signals A, B, C, and D with fair precision in a central area of 2° × 2°. It is possible to obtain a transformation matrix **V** and calculate the horizontal and vertical directions of gaze from the four quadrant signals by means of a linear transformation and subsequent correction, after calibration for each individual subject studied. The correction matrices are based on resampling the linear estimate $[X, Y] = \mathbf{AV}$ with the goal of reversing the initial error and have proved to be efficient in this application.

The major advantage of this eye-tracking method is that it uses true information coming from the fovea,

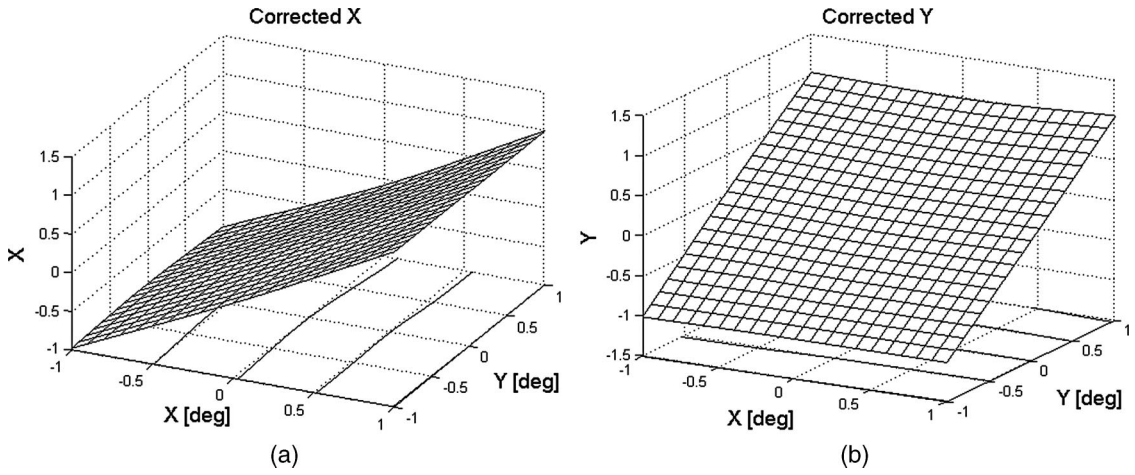

Fig. 8. Eye tracking with human data: the corrected signals for (a) X and (b) Y after XY matrix correction.

rather than reflections from other structures, to identify the direction of foveal gaze. We believe that a sensor based on true foveal fixation, despite all the difficulties described in this article, would be superior to common commercial eye trackers employing the corneal light reflex and/or pupil information. Other currently used methods are either invasive, restrict head movement strongly, or provide output referenced to head coordinates only. In most studies of eye position, it is the projection of the fovea onto the environment (fixation) that is of interest. Our method can detect true foveal position. Most other techniques measure the orientation of the globe (eye position), requiring a calibration step to avoid discrepancy between inferred and true foveal fixation in certain eye conditions (e.g., eccentric pupil). The present measuring principle, although also requiring calibration, is based on autoconjugacy of the retina with the light source and with the detector and permits relatively free movement of the head.[19]

The accuracy was better than 0.11° for X and 0.08° for Y (respectively, 5.5% and 4.0%, relative to the field size of 2° × 2°). Existing eye trackers offer visual ranges of 30°–40° at accuracies varying between 0.005° (Ref. 9) and 1°–2° (Applied Science Laboratories, Model 310). The speed of our device is defined by acquiring an averaged analog measurement from four points, applying a matrix multiplication [Eq. (1)], and then performing the correction by means of table lookup or interpolation [Eq. (4)]. In the most robust application, which was synchronous averaging of 28 measurement cycles (7.14 ms each) within a 200 ms epoch, with interpolation during correction, a gaze-detection process took less than 250 ms (4 Hz). Decreasing the duration of the measurement epoch to 4 ms while increasing the laser modulation frequency to 1 kHz increased measurement speed to 200 Hz and more, without significantly sacrificing precision. This is comparable to the speed of the fastest eye trackers on the market. Although slowed down by the signal averaging needed to overcome significant background noise in the present implementation, this method is simpler and could potentially be made faster than many eye trackers built around CMOS image sensors, because it works on only four channels. High frame rate CMOS eye-tracking devices have indeed been reported to achieve sample-and-process rates of the order of 30–400 Hz, but at the cost of excessive electronic hardware. For example, such a high-end application referenced earlier,[9] in addition to complex hardware, employs a sophisticated head unit with adjusters and a molded facemask to minimize head-to-device slippage while using pupil information only.

An eye-tracking device of the type reported in this paper will need individual eye-gaze calibration as described in Subsection 3.B in order to compute the transformation matrix **V** and the correction matrices for each subject. This renders the method somewhat cumbersome for some applications. At the same time, most laboratory and commercial eye trackers currently use some form of gaze-direction calibration.[2,4,7–10,30]

A point of special concern is the influence of corneal birefringence on the precision of this method. As pointed out before, the functioning of this device is based on the birefringence of the nerve fibers surrounding the fovea, i.e., on the property of these fibers to change the state of polarization. However, besides the fovea, the light going into and coming out of the eye also passes through the birefringent cornea, which behaves as a retarder, in general causing some rotation of the bow-tie pattern being analyzed. In addition, the retardance and azimuth of the cornea can vary quite significantly from patient to patient.[31,32] Using a computer model described elsewhere,[18] we studied the influence of corneal birefringence on the orientation of the bow-tie pattern with respect to the four spots of light in this particular device.[24] This analysis showed (based on the data published by Knighton and Huang[31]) that, for the majority of the 143 human eyes they studied, the orientation of our bow-tie axis is between 30° and 50°. The model described in Subsection 2.B and the correction algorithm presented in Subsection 2.E completely eliminate the influence of this rotation, because the computed transformation matrix **V** and the correction matrices **COR_X** and **COR_Y** are different in the case of a rotated bow tie. This automatically compensates for any rotation of the bow tie.

A limitation of this eye-tracking method is the relatively small visual field (2° × 2°) in which it can be reliably used. This restriction comes partially from the size and the imperfect shape of the bow-tie light intensity pattern and from the simplified assumption that the four signals from the four quadrants of the photodetector can be converted to x and y coordinates of gaze by using a straightforward linear transformation [(Eqs. (2) and (3)]. The correction as described in Subsection 2.E greatly improves accuracy. Its limitations are related mainly to the interpolation algorithm used to obtain the correction matrices after calibration and to the real-time interpolation needed to produce the output from the estimated x–y values and the nearest correction matrix control points.

The eye-tracking range can be significantly increased by using the retinal nerve fiber layer (RNFL), which creates a similar bow-tie pattern of polarization states around the optic disk in polarized light reflected from the fundus. The RNLF pattern spans approximately 20°, compared with the 5°–6° covered by the Henle fibers surrounding the fovea and used in the present device.

A substantial difficulty with the implementation of the method used in the present study is the low signal-to-noise ratio of roughly 0.1 due to light reflected from the lids, sclera, and cornea. This problem was largely solved by using time-synchronous averaging of a number of measurement cycles. Increasing the number of averaged cycles with the purpose of achieving more stable readings would limit even further the time resolution of the directional eye fixation sensor. Clearly, increasing the signal-to-noise ratio is necessary. This could be achieved by masking the face and sclera with a low-reflective material such as

black felt. Such a mask in our tests decreased the background signal from facial reflections approximately threefold and greatly improved measurement stability of the eye tracker. Another way to reduce the effect of the reflections from the sclera, cornea, and face would be to modify the system so that the four light spots are fired sequentially, rather than simultaneously, i.e., by using four truly separate laser point sources instead of one laser diode with a multifaceted prism. This would decrease background noise nearly four times and reduce the number of cycles needed to be acquired and averaged. Indeed, a rapidly fired array of 8 or 16 light spots would simulate a scanning motion and provide the noise-reduction advantages of a scanned system without need for moving parts, perhaps eliminating the need for signal averaging.

Head tilts and ocular torsion appearing after calibration would produce artifacts that our device is not designed to accommodate. Future work aimed at calibration at different tilt angles and estimating a change of angle ψ in real time may solve this problem. Possible media opacities, such as corneal scars or partial cataracts, would also adversely influence precision.

Another factor that potentially may deteriorate the precision of this device is small pupil size. Since the eye tracker uses a double-pass method, pupil constriction after calculation of $\mathbf{V}$ and the correction matrices may play a negative role in the precision of eye-position detection. We have successfully tested the device in a low-light environment only. The impact of changing the level of the room lights has yet to be studied. Yet again, some existing eye-tracking systems were reported to be used in dimly lit laboratories.[11,14] Systems employing an infrared source of eye illumination usually perform much better at low ambient light levels. However, accommodation also induces pupil constriction, and accommodation may occur during demanding visual tasks that might require eye tracking.

5. Conclusion

We have demonstrated the feasibility of an eye tracker that utilizes birefringence-based foveal position detection. Our method and device can be used for remote, noninvasive, continuous monitoring of foveal fixation within $\pm 1°$ in both the horizontal and the vertical directions, at a relatively slow speed. The field can potentially be expanded by using other birefringence structures of the fundus of the eye such as the retinal nerve fiber layer around the optic disk. We believe that reading rates of several hundred measurements/s are achievable with this method. The approach has potential use in vision diagnostics, remote control applications, security systems, aids for disabled people, biometrics, vehicular technologies, computer gaming, and other areas. It requires no rigid head fixation and needs no head-mounted appliances.

This work was supported by awards from Research to Prevent Blindness and the Alcon Research Institute and by NIH grant EY12883. David Kays from the Wilmer Eye Institute provided technical assistance.

References

1. H. Collewijn, F. van der Mark, and T. C. Jansen, "Precise recording of human eye movements," Vision Res. **15,** 447–450 (1975).
2. E. Paperno and D. Semyonov, "A new method for eye location tracking," IEEE Trans. Biomed. Eng. **50,** 1174–1179 (2003).
3. J. Merchant, "Laboratory Oculometer," Honeywell, Radiation Center/Electronics Research Center, NASA, Lexington, Mass. (1968).
4. K. Hartnegg and B. Fischer, "A turn-key transportable eye-tracking instrument for clinical assessment," Behav. Res. Methods Instrum. Comput. **34,** 625–629 (2002).
5. T. N. Cornsweet and H. D. Crane, "Accurate two-dimensional eye tracker using first and fourth Purkinje images," J. Opt. Soc. Am. **63,** 921–928 (1973).
6. M. Eizenman, R. C. Frecker, and P. E. Hallett, "Precise noncontacting measurement of eye movements using the corneal reflex," Vision Res. **24,** 167–174 (1984).
7. J. P. Reulen, J. T. Marcus, D. Koops, F. R. de Vries, G. Tiesinga, K. Boshuizen, and J. E. Bos, "Precise recording of eye movement: the IRIS technique. Part 1," Med. Biol. Eng. Comput. **26,** 20–26 (1988).
8. K. Irie, B. A. Wilson, R. D. Jones, P. J. Bones, and T. J. Anderson, "A laser-based eye-tracking system," Behav. Res. Methods Instrum. Comput. **34,** 561–572 (2002).
9. A. H. Clarke, J. Ditterich, K. Druen, U. Schonfeld, and C. Steineke, "Using high frame rate CMOS sensors for three-dimensional eye tracking," Behav. Res. Methods Instrum. Comput. **34,** 549–560 (2002).
10. J. S. Stahl, A. M. van Alphen, and C. I. De Zeeuw, "A comparison of video and magnetic search coil recordings of mouse eye movements," J Neurosci. Methods **99,** 101–110 (2000).
11. F. Schaeffel, "Kappa and Hirschberg ratio measured with an automated video gaze tracker," Optom. Vision Sci. **79,** 329–334 (2002).
12. A. Talukder, J.-M. Morookian, S. Monacos, R. Lam, C. LeBaw, and J. L. Lambert, "Eye-tracking architecture for biometrics and remote monitoring," Appl. Opt. **44,** 693–700 (2005).
13. C. Mello-Thoms, C. Britton, G. Abrams, C. Hakim, R. Shah, L. Hardesty, G. Maitz, and D. Gur, "Head-mounted versus remote eye tracking of radiologists searching for breast cancer: a comparison," Acad. Radiol. **13,** 203–209 (2006).
14. M. S. Salman, J. A. Sharpe, M. Eizenman, L. Lillakas, C. Westall, T. To, M. Dennis, and M. J. Steinbach, "Saccades in children," Vision Res. **46,** 1432–1439 (2006).
15. S. Duke-Elder, N. Ashton, R. J. H. Smith, and M. Lederman, "Entoptic Observations," in *The Foundations of Ophthalmology, System of Ophthalmology* (C. V. Mosby, 1964), Chap. 15.
16. H. B. Klein Brink and G. J. van Blokland, "Birefringence of the human foveal area assessed *in vivo* with Mueller-matrix ellipsometry," J. Opt. Soc. Am. A **5,** 49–57 (1988).
17. A. W. Dreher, K. Reiter, and R. N. Weinreb, "Spatially resolved birefringence of the retinal nerve fiber layer assessed with a retinal laser ellipsometer," Appl. Opt. **31,** 3730–3735 (1992).
18. D. G. Hunter, J. C. Sandruck, S. Sau, S. N. Patel, and D. L. Guyton, "Mathematical modeling of retinal birefringence scanning," J. Opt. Soc. Am. A **16,** 2103–2111 (1999).
19. D. G. Hunter, S. N. Patel, and D. L. Guyton, "Automated detection of foveal fixation by use of retinal birefringence scanning," Appl. Opt. **38,** 1273–1279 (1999).
20. D. L. Guyton, D. G. Hunter, S. N. Patel, J. C. Sandruck, and R. L. Fry, "Eye fixation monitor and tracker," U.S. Patent 6,027,216 (22 February 2000).

21. D. G. Hunter, A. S. Shah, S. Sau, D. Nassif, and D. L. Guyton, "Automated detection of ocular alignment with binocular retinal birefringence scanning," Appl. Opt. **42,** 3047–3053 (2003).
22. D. Nassif, B. Gramatikov, D. Guyton, and D. Hunter, "Pediatric vision screening using binocular retinal birefringence scanning," *Ophthalmic Technologies XIII,* Proc. SPIE **4951,** 9–20 (2003).
23. D. G. Hunter, D. S. Nassif, N. V. Piskun, R. Winsor, B. I. Gramatikov, and D. L. Guyton, "Pediatric vision screener 1: instrument design and operation," J. Biomed. Opt. **9,** 1363–1368 (2004).
24. B. I. Gramatikov, O. H. Y. Zalloum, Y. K. Wu, D. G. Hunter, and D. L. Guyton, "Birefringence-based eye fixation monitor with no moving parts," J. Biomed. Opt. **11,** 034025 (2006).
25. D. Sliney and M. Wolbarsht, *Safety with Lasers and Other Optical Sources* (Plenum, 1980).
26. W. A. Shurcliff, *Polarized Light: Production and Use* (Harvard U. Press, 1962).
27. D. S. Klieger, J. W. Lewis, and C. E. Randall, *Polarized Light in Optics and Spectroscopy* (Academic, 1990).
28. S. N. Patel, "Analysis of foveal birefringence to monitor eye fixation," M. S. thesis (Johns Hopkins U. Press, 1995).
29. D. T. Sandwell, "Biharmonic spline interpolation of GEOS-3 and SEASAT altimeter data," Geophys. Res. Lett. **2,** 139–142 (1987).
30. J. N. Van der Geest and M. A. Frens, "Recording eye movements with video-oculography and scleral search coils: a direct comparison of two methods," J Neurosci. Methods **114,** 185–195 (2002).
31. R. W. Knighton and X. R. Huang, "Linear birefringence of the central human cornea," Invest. Ophthalmol. Visual. Sci. **43,** 82–86 (2002).
32. R. N. Weinreb, C. Bowd, D. S. Greenfield, and L. M. Zangwill, "Measurement of the magnitude and axis of corneal polarization with scanning laser polarimetry," Arch. Ophthalmol. (Chicago) **120,** 901–906 (2002).